

Chapter 15

In Situ Sulfur Speciation Using Au/Hg Microelectrodes as an Aid to Microbial Characterization of an Intertidal Salt Marsh Microbial Mat

Brian T. Glazer, S. Craig Cary, Laura Hohmann, and George W. Luther, III

College of Marine Studies, University of Delaware, 700 Pilottown Road,
Lewes, DE 19958

Sulfur speciation was determined *in situ* in a mid-Atlantic salt marsh microbial mat using a solid-state gold-amalgam voltammetric microelectrode. Chemical constituents were measured in real time with no sample manipulation or processing. A transition from O_2 to partially oxidized sulfur species (polysulfides, thiosulfate, and elemental sulfur) to H_2S was detected through the mat. Metal oxidation (Fe and Mn) of hydrogen sulfide did not occur in the mat, where microbially mediated processes are responsible for H_2S oxidation. The ~7 mm thick mat was frozen *in situ* and cryomicrotome-sectioned into 20-micron sections for visual and molecular biological analyses of the microbial community. The upper 3.16 mm of the mat was dominated by a filamentous morphotype while the lower 3.59 mm was dominated by a rod morphotype. The shift between the two morphologies corresponded to a zone of transition between $S_8/S_2O_3^{2-}$ and S_x^{2-} .

Introduction

It has been the aim of many researchers to attempt to identify bacterial processes and associated geochemical gradients in microbial environments. Dense microbial mats provide one of the best environments for such studies, as they exhibit sharp gradients of redox species and they are relatively easy to sample in the field and manipulate in the lab (1). Specifically, much work has been dedicated to cyanobacterial mat communities living in intertidal coastal sediments, marine salterns, hypersaline ponds and lakes, thermal springs, dry and hot deserts and Antarctic lakes (1-3). These benthic microbial communities often develop a stratification of diverse chemical and biological species in response to periodic stressors and environmental variations including irradiance, tidal inundation, desiccation, temperature fluctuation, and salinity variations (1,2).

The use of microelectrodes in these complex microbial communities has allowed for accurate, fine-scale determination of chemical redox gradients for parameters such as pH, O₂, CO₂, and H₂S (4, 6-8, 48, 49). However, until recently advances have been limited by the inability to produce simultaneous *in situ* measurements and differentiations between varying chemical species (4-8). The solid-state gold-amalgam (Au/Hg) electrode described by Brendel and Luther (9) enables simultaneous measurements of multiple redox species *in situ*, and has recently been shown to differentiate between a variety of sulfur species (10, 11).

Here we examined a microbial mat found in a salt marsh environment that produces reduced sulfur species from sediments below the mat. Such sulfur species can then be oxidized back to sulfate as they diffuse upward, by oxygen, iron (III), and manganese (III, IV) compounds (12-16), with and without microbial intervention. Oxidation of sulfide can frequently result in the formation of intermediate compounds such as elemental sulfur, polysulfides and thiosulfate, which can be utilized by bacteria (17) or may react with metals (18) and organic compounds (19, 20). Since the sulfur cycle is so dominant in marine systems, with sulfate being the dominant electron acceptor in marine sediments, it is essential to attempt to better understand the dynamics of the complex reactions involved and couple them to the organisms living in those gradients.

In this work we describe the *in situ* application of voltammetric techniques using gold-amalgam microelectrodes to measure microscale vertical variation of chemical species in a seasonal salt marsh microbial mat. We quantify the presence or report the absence of the important chemical redox species, and characterize the microbial consortia using fluorescent microscopy and molecular techniques, with sub-millimeter resolution.

Experimental methods

Electrochemical techniques

A standard three-electrode cell was used in all electrochemical measurements. The working electrode was a gold amalgam (Au/Hg) electrode of 0.1 mm diameter made in 5 mm glass drawn to 0.2-0.3 mm and sealed with epoxy as described by Brendel and Luther (9). Counter (Pt) and reference (Ag/AgCl) electrodes, each of 0.5 mm diameter, were made in commercially available PEEK (polyethyl ether ketone) tubing.

For the voltammetric measurements, the voltage range scanned was from -0.1 V to -2.0 V. In linear sweep voltammetry (LSV) and cyclic voltammetry (CV) the scan rate was 200, 500, or 1000 mVs⁻¹, depending on targeted chemical species. The parameters for square wave voltammetry (SWV) were as follows: pulse height, 24 mV; step increment, 1 mV; frequency, 100 Hz; scan rate, 200 mVs⁻¹. LSV and CV were used to measure oxygen and sulfur species, while SWV was employed for detection of metal redox species. Electrochemically conditioning the electrode between scans removed any chemical species from the surface of the electrode, restoring it for the next measurement. To remove any deposited Fe or Mn the working electrode was conditioned at a potential of -0.1V for 10s (9). Prior to field excursions, standard curves were produced for O₂, Mn, and sulfur species, as described previously (9, 10).

In July of 2000, a portable Analytical Instruments System (AIS) DLK 100(a) voltammetric analyzer was taken to a large panne (greater than 5 m²) in Great Marsh, Delaware for *in situ* chemical analyses of a microbial mat. Mats in this location develop on a temporary basis, and can be destroyed by rain, tidal cycles, and dessication. An attempt was made to select a relatively flat, level section of mat with a few centimeters of overlying water for sampling. Measurements were made at approximately noon on a sunny day. The gold amalgam electrode was inserted into the water and into the mat with a manually controlled three-axis Narishige micromanipulator in 0.5 mm increments, and voltammetric scans were produced at each depth in triplicate. To prevent sulfidic fouling, counter and reference electrodes were placed in the water overlying the mat so they would not be in contact with the mat, sediment, or sulfide zone. Salinity and temperature of the overlying water were measured in order to calculate O₂ saturation.

Microbial mat samples

Immediately following voltammetric measurements from the deepest point of the profile, the electrochemical equipment was carefully extracted and a core of the mat was taken using a copper tube with a diameter of 1.6 cm. The mat sample was then immediately pushed through the core tube and plunged into liquid propane. A wide-mouth dewar containing dry ice and a copper receptacle was transported to the field in a small cooler packed with insulating closed-cell foam. Prior to removing the core from the mat, approximately 15 ml of liquid propane was allowed to accumulate in the copper reservoir by inverting a portable, disposable propane cartridge with a modified torch head attachment. This proved to be an inexpensive, efficient method to immediately freeze the mat in the field. Both freezing the mat sample in the field and the use of liquid propane to ensure rapid freezing and small ice crystal formation were expected to minimize distortion and accurately preserve the original spatial orientation of the microbial community (21). The mat sample was kept frozen and sectioned into 20 μm slices with a Spencer 830-C Cryo-Cut cryostat microtome. Three of these 20 μm sections were pooled for molecular analyses at 0.25 mm increments throughout the 7 mm mat. Twenty- μm sections were also removed at 1.75 mm increments and mounted on glass microscope slides to provide for fluorescent microscopic analysis. In addition to the single mat core described above, a replicate core was taken for a preliminary DNA extraction comparison experiment.

Fluorescent microscopy

Sections mounted on microscope slides were stained with DAPI (22) to visualize section constituents and minimize non-specific background staining (23, 24). Images were resolved on an Olympus Provis AX70 microscope using a 100x objective lens and captured with a CTD camera with effective pixel size of 0.074 microns. The filter used to visualize the DAPI stain was a Chroma 3100 band pass filter.

DNA extraction

Typically marsh sediments contain humics and tannins that can inhibit enzymes used in molecular biological analyses. In an effort to optimize methodology and minimize effects of sediment contamination we compared two differing methods of DNA extraction. Hexadecyltrimethyl ammonium bromide (CTAB) and an Isoquick DNA extraction kit (Isoquick, Inc.), were compared

using mat material from an area of mat adjacent to where *in situ* electrochemical analyses took place. Each tube of thawed sample sections received 500 μL of CTAB extraction buffer (100 mM tris-HCl, 1.4 M NaCl, 0.4% B-ME, 1% PVP, 2% CTAB, and 20 mM EDTA) preheated to 60°C. Tubes were vortexed and heated to 60°C for 15 minutes. Upon cooling, 500 μL of chloroform:isoamyl alcohol (25:1) was added to the mixture, mixed, and rocked gently for 20 minutes. Following 15 minutes of centrifugation at 12,500 rpm with a Kompspin PC-18 micro table top centrifuge (Composite Rotor, Inc.), the extraction buffer phase was transferred to a clean tube. 5 M sodium chloride (0.5x of recovered volume) and 100% isopropyl alcohol (1x of recovered volume) was added to the tubes, followed by 1 hour freezing at -80°C to precipitate DNA. Tubes were thawed, centrifuged at 12,500 rpm for 15 minutes, and the DNA pellet was washed with cold 70% ethanol. The isolated pellet was then resuspended in distilled water and stored at -20°C for analyses. Replicate samples were subjected to the Isoquick DNA extraction kit (Isoquick, Inc.) according to the manufacturer's instructions.

DNA obtained from both methods was analyzed on a spectrophotometer to assess DNA purity and concentration (25) and resolved on a 1% Seakem agarose gel. These preparations were subsequently used as template DNA in the polymerase chain reaction (PCR) (26).

PCR amplification

The variable V3 region of 16S rDNA was amplified in the PCR (26) with primers designed for conserved regions of the 16S rRNA genes (27). The primer nucleotide names and sequences are as follows: 338FGC, 5'-CCTACGGGAGGCAGCAG-3', with an additional 40-nucleotide GC-rich sequence (GC clamp) at its 5' end; and 519RC, 5'-ATTACCGCGGCTGCTGG-3', as described in Muyzer et al. (28). Polymerase chain reaction amplification followed the procedure of Muyzer et al. (28). Briefly, amplification was performed on an MJ Research PTC-150 Minicycler™ (MJ Research, Inc., Watertown, MA) with a Hot Bonnet™ heated lid in 50 μL reactions with final concentrations as follows: approximately 50 ng of template genomic DNA, 0.4 μM of each of the primers, 0.2 mM (each) deoxyribonucleoside triphosphate, 1x Promega PCR buffer, and 1.5 mM MgCl_2 . *Taq* DNA polymerase addition followed the hot start technique described by D'Aquila et al., (45) to minimize nonspecific annealing of primers to non-target DNA template. The PCR also incorporated the touchdown technique described by Muyzer et al., (28), lowering annealing temperature by 1 °C every second cycle until 55 °C to reduce the formation of spurious by-products during the amplification process. Primer extension was carried out at 72 °C for 1 minute. Amplification products were

analyzed in 1% Seakem gels stained with ethidium bromide (EtBr) (1 mg/mL) and resolved with UV light.

DGGE analysis

Denaturing gradient gel electrophoresis was performed with a BioRad Dcode™ Universal Mutation Detection System, as described in Fischer et al. (29). Seventeen μL of PCR product was added to 17 μL of loading buffer, and subsequently loaded directly onto 8% polyacrylamide gels (37.5:1 ratio of acrylamide-bisacrylamide) poured with a 25%-55% gradient of denaturant (100% denaturant is 7M urea, 40% deionized formamide). Electrophoresis was performed at a constant voltage of 130 V and temperature of 60°C for 4 hours in 0.5X TAE buffer (40 mM Tris base, 20 mM sodium acetate, 1 mM EDTA). Gels were stained with EtBr (1 mg/ml) for 15 minutes and destained in deionized water for 15 minutes. Bands were then resolved on a Fisher Biotech Electrophoresis Systems Variable Intensity Transilluminator and digital images were captured with an Alpha Imager 2000 Documentation and Analysis System (AlphaInnotech Corp., San Leandro, CA).

Results and discussion

Sulfur speciation

Table I shows many of the redox compounds and ions including some of the sulfur species measurable by the Au/Hg electrode. Sulfide oxidation results in formation of polysulfides, elemental sulfur, thiosulfate, sulfite and polythionates (e.g. tetrathionate) in lab studies (12-16) but the presence of such intermediates has been confirmed in few field studies (10, 30-34). Sulfite, can be measured (30) at pH values <6, which are not common in microbial mats or sediments, where pH values are normally > 7. All of the sulfur species we measured gave a single peak except for polysulfides. At slow scan rates, H_2S , S_8 , and polysulfides overlap to give one peak at about -0.60V , and the sum of their contributions is termed S_{red} (10, 30-35). However, S_x^{2-} are unique because they exist in two oxidation states and it is possible to discriminate each oxidation state with fast potential scans (10). At a potential more positive than -0.6V , S_x^{2-} reacts to form an HgS_x species at the Au/Hg electrode, which is an electrochemical oxidation of the Hg. Scanning negatively then results in HgS_x reduction to Hg and S_x^{2-} overlapping with, but slightly more positive than H_2S and S_8 . The $(x-1)\text{S}^0$ atoms

Table I. Measurable redox reactions occurring at the 0.1mm Au/Hg electrode surface vs. the 0.5mm Ag/AgCl reference electrode. Oxygen data were collected by linear sweep voltammetry at a scan rate of 500 mVs⁻¹.

Cyclic voltammetry was employed in the absence of oxygen to better measure sulfur species, using 200, 500, or 1000 mVs⁻¹. Square wave voltammetry was used at 200 mVs⁻¹ for detection of metal redox species. Potentials can vary with scan rate and concentration. When applying potential from a positive to negative scan direction, sulfide and S(0) react in a two step process: adsorption onto the Hg surface, and reduction of the HgS film. Polysulfides react in a three step process: adsorption onto the Hg surface, reduction of the HgS_x film, and reduction of the S(0) in the polysulfide. Increasing the scan rate separates electrode reactions 4b and 4c into two peaks because reaction 4c is an irreversible process. Increasing scan rate shifts this signal (36). MDL-minimum detection limit

		E _p (V)	MDL (μM)
1a	$O_2 + 2H^+ + 2e^- \rightarrow H_2O_2$	-0.30	2
1b	$H_2O_2 + 2H^+ + 2e^- \rightarrow H_2O$	-1.3	2
2a	$HS^- + Hg \rightarrow HgS + H^+ + 2e^-$	<-0.60	
2b	$HgS + H^+ + 2e^- \leftrightarrow HS^- + Hg$	~-0.60	<0.2
3a	$S(0) + Hg \rightarrow HgS$	<-0.60	
3b	$HgS + H^+ + 2e^- \leftrightarrow HS^- + Hg$	~-0.60	<0.2
4a	$Hg + S_x^{2-} \rightarrow HgS_x + 2e^-$	<-0.60	
4b	$HgS_x + 2e^- \leftrightarrow Hg + S_x^{2-}$	~-0.60	<0.2
4c	$S_x^{2-} + xH^+ + (2x-2)e^- \rightarrow xHS^-$	~-0.60	<0.2
5	$2 RSH \leftrightarrow Hg(SR)_2 + 2H^+ + 2e^-$	>H ₂ S/ HS ⁻	
6	$2 S_2O_3^{2-} + Hg \leftrightarrow Hg(S_2O_3)_2^{2-} + 2e^-$	-0.15	16
7	$S_4O_6^{2-} + 2e^- \rightarrow 2 S_2O_3^{2-}$	-0.45	15
8	$FeS + 2e^- + H^+ \rightarrow Fe(Hg) + HS^-$	-1.1	molecular species
9	$Fe^{2+} + Hg + 2e^- \leftrightarrow Fe(Hg)$	-1.43	15
10	$Fe^{3+} + e^- \leftrightarrow Fe^{2+}$	-0.2 to -0.9	molecular species

are reduced to sulfide at a slightly more negative potential. Since the reduction of S^0 atoms in S_x^{2-} is an irreversible process, an increase in scan rate results in a shift of the peak to a more negative potential, permitting a visual separation of the HgS_x reduction from the S_8 reduction (Table I, eqs 4a-c, and Figure 1D) (10, 36). The peaks can be resolved at 1000 mVs^{-1} .

Microelectrode gradients

Figure 1 depicts representative voltammograms taken from the profiling of the microbial mat. Scan A, 4 mm above the mat in the overlying water, shows the presence of oxygen, whereas Scan B shows a significant signal due to H_2O_2 at 3 mm above the mat surface, masking any signal due to oxygen (detection limit of $2\mu\text{M}$). The magnitude of the H_2O_2 signal is typically equal to that of the oxygen signal because at the electrode surface ambient O_2 reduces to H_2O_2 (Table I, eqs 1a-b), which in turn reduces to H_2O . Here however, there is an excess of H_2O_2 which has also been shown to exist in significant quantities in biofilms (37). Scan C, at 2 mm below the surface of the mat, shows 2 peaks. The first, at $E_{1/2}=-0.15\text{ V}$ represents thiosulfate, and the second, at $E_{1/2}=-0.60\text{ V}$ represents S_{red} . The single peak at -0.6 V (visible at the fast scan rate of 1000 mVs^{-1}) indicates that polysulfides are not present as part of S_{red} . Thus, S_{red} is, in this case, composed of soluble S_8 because this upper part of the mat is more oxidized due to the oxygen gradient. At 5 mm below the mat surface, Scan D shows a clear double peak at $E_{1/2}=-0.58\text{ V}$ and -0.68 V , indicative of polysulfide formation. The more positive signal is due to S^{2-} sulfur from H_2S and S_x^{2-} and the more negative signal is due to S^0 sulfur from S_x^{2-} . As the bottom of the mat is passed and the underlying sediment penetrated, Scan E shows only 1 peak at $E_{1/2}=-0.58\text{ V}$, indicating only H_2S/HS^- is present. Trace amounts of FeS are noted in Scan E and other scans deeper into the mat (data not presented). No scans gave evidence of dissolved Fe or Mn in the mat (detection limit of $10\mu\text{M}$).

Figure 2 shows a concentration versus depth profile of oxygen and sulfur species into the mat. The O_2 profile is typical for microbial mats (3, 5, 38, 39). Daytime oxygen levels reach a maximum ($\sim 200\%$ saturation) in the water column above the mat/water interface, characteristic of an oxygenic photosynthetic microenvironment. Concentrations of H_2O_2 , an intermediate in O_2 formation via water splitting, were observed just above the mat surface. Previous microelectrode studies using membrane electrodes could not determine

if H_2O_2 was present, but solid-state microelectrodes used in biofilm work have reported the presence of H_2O_2 (37).

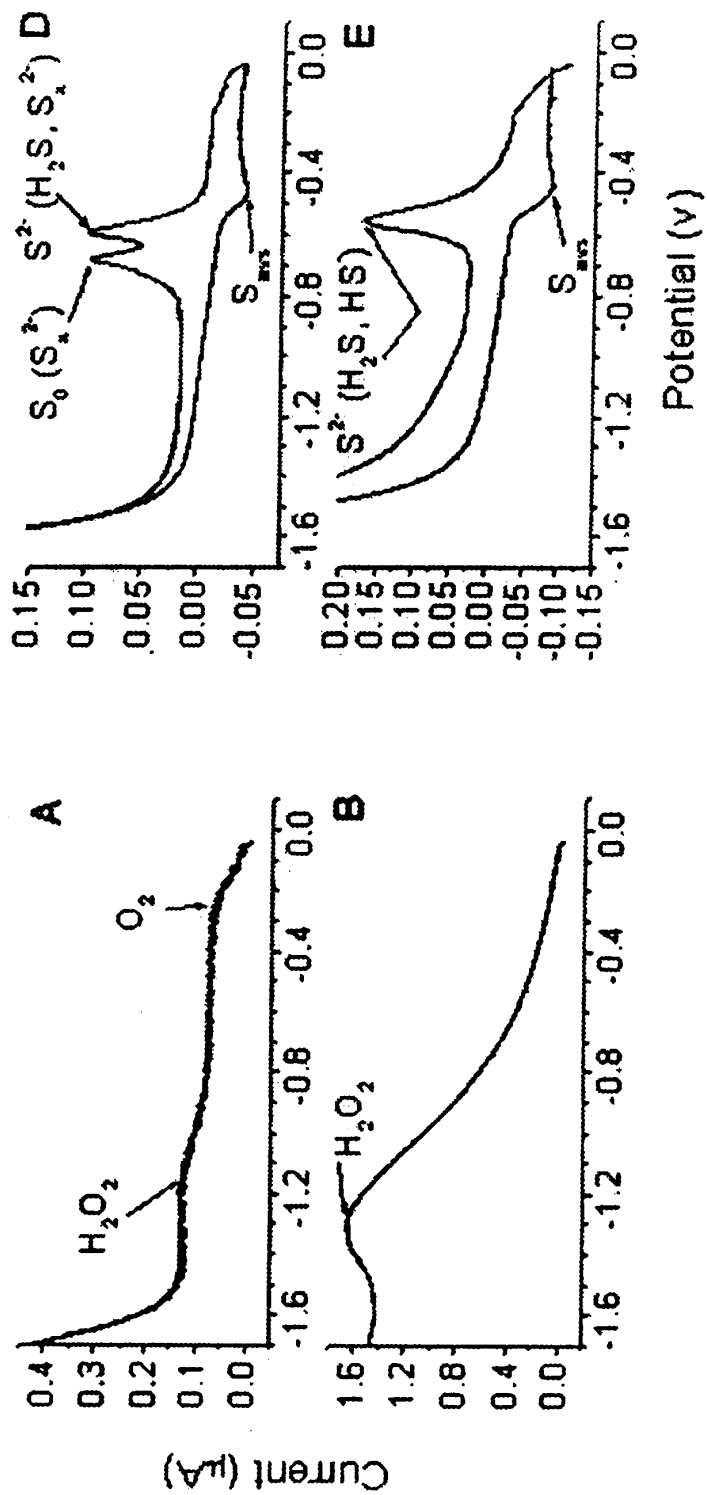
While colorimetric analyses (5, 38, 39) have been employed to measure sulfur species such as thiosulfate, tetrathionate and polysulfides in lab cultures and processed microbial mat cores from thick films that could be cut and analyzed, this is the first report of *in situ* sulfur species determination other than H_2S in a microbial mat. Their occurrences were as predicted, and the overall oxidation appears to be primarily due to biological processes, as no metals (Fe, Mn) which could oxidize sulfide were detected, and O_2 did not co-exist with H_2S .

Fluorescent microscopy

Figure 3 depicts four images typical of 20-micron DAPI-stained sections from within the mat. Picture A is of a 20-micron section taken from 1.20 mm below the mat surface that clearly shows the dominance of sheathed bundles of cells, characteristic of oxygenic photosynthetic cyanobacteria. Picture B shows similar community composition 4.80 mm below the mat surface. Depicted in Picture C, 6.34 mm below the mat surface, is a markedly different community where all sheathed cells are absent, and smaller rods & cocci are dominant. This suggests a striking shift in the community composition occurred between 4.80 and 6.34 mm below the mat surface. It is likely that the shift in dominant organisms is in response to differing metabolic requirements, allowing for reduced substrates diffusing upward from the permanently anoxic sediments to act as electron donors. Picture D, taken from 7.23 mm below the surface represents the bottom-most microbial constituents of the mat and further suggests a morphological gradient exists from sheathed cells at the top, oxygenated portion of the mat to smaller rods and cocci in the deeper, more sulfidic zone. Other studies have shown that cyanobacteria, purple sulfur bacteria, and sulfate-reducing bacteria are ultimately responsible for the steep and fluctuating chemical gradients (1).

Molecular analyses

The two methods we compared for DNA extraction yielded differing results. Figure 4 illustrates typical results of extractions performed using CTAB versus extractions performed with an Isoquick kit. The reproducible streaking and multiple band formation in the CTAB extracts were probably not attributable to initial template concentrations, which ranged from 200-800 ng/ μL and were



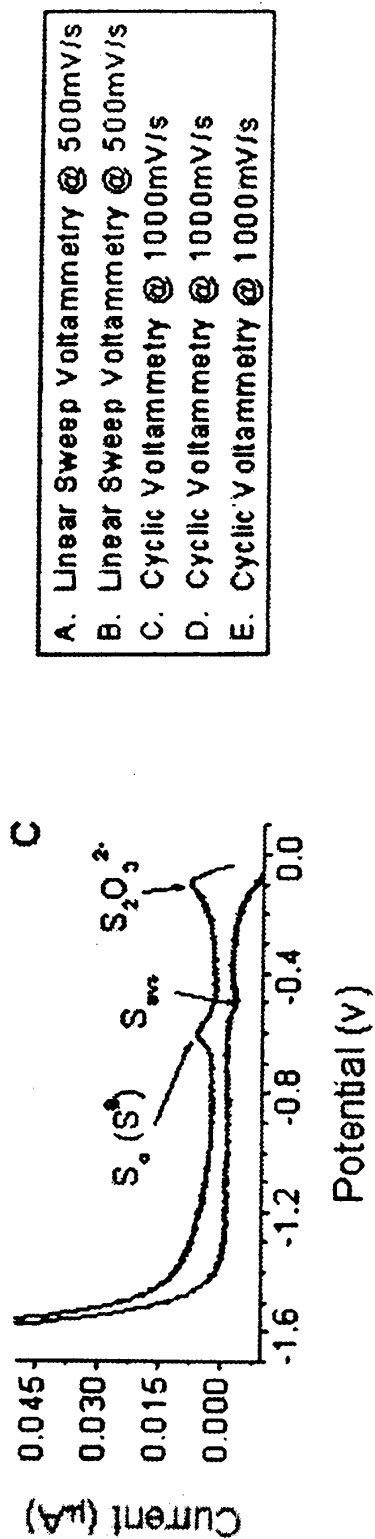


Figure 1. Representative voltammetric scans from varying depths in the mat. A is from 5 mm above the mat surface in the overlying water, B is 3 mm above the mat surface, C is 2 mm below the mat surface, D is 4 mm below the mat surface, and E is 7.55 mm below the mat surface, in the underlying sediment.

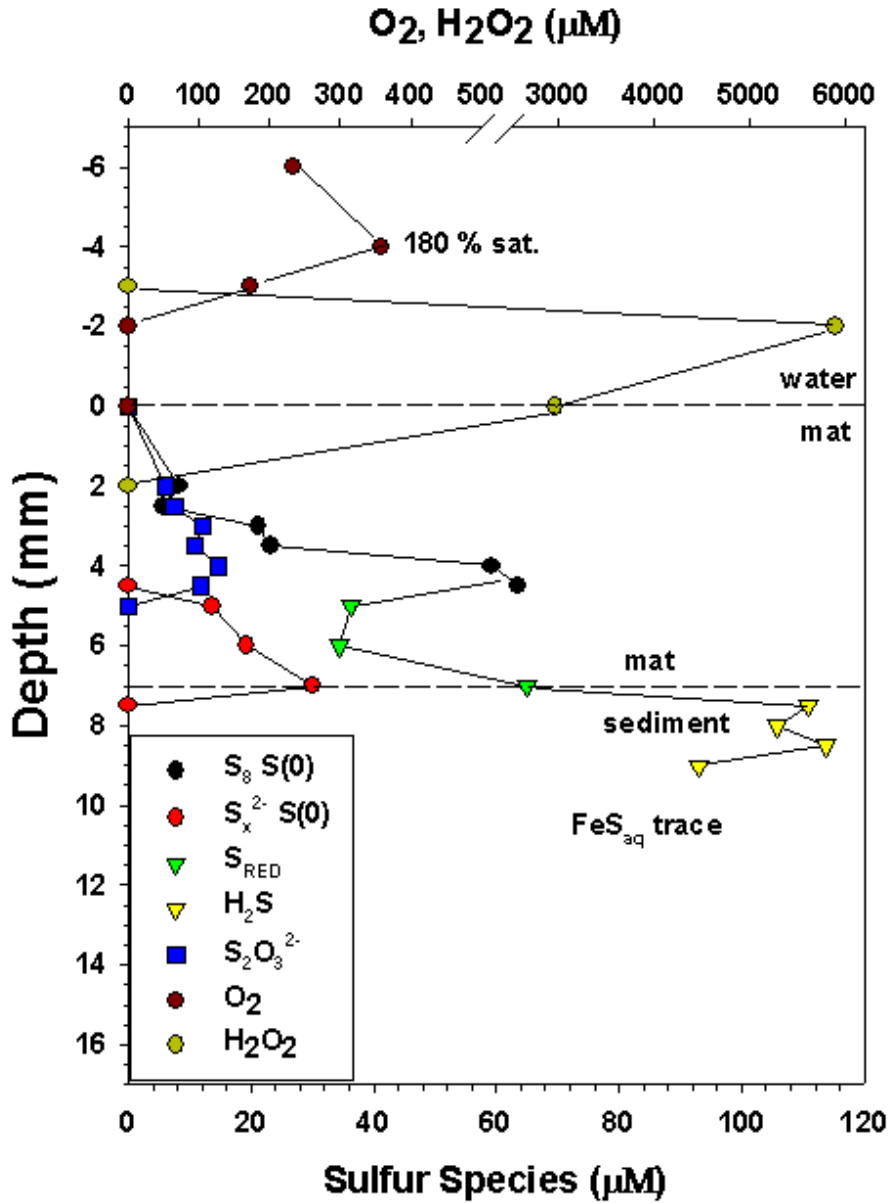


Figure 2. Profile of all chemical components measured in the mat. Once a chemical species is no longer detected it is not plotted. S_{red} represents the sum of all sulfur in the 2- oxidation state from polysulfides and H_2S/HS^- and in the 0 oxidation state from S_8 . Note that data points are connected in the figure to show the transition from S_8 to S_x^{2-} to H_2S .

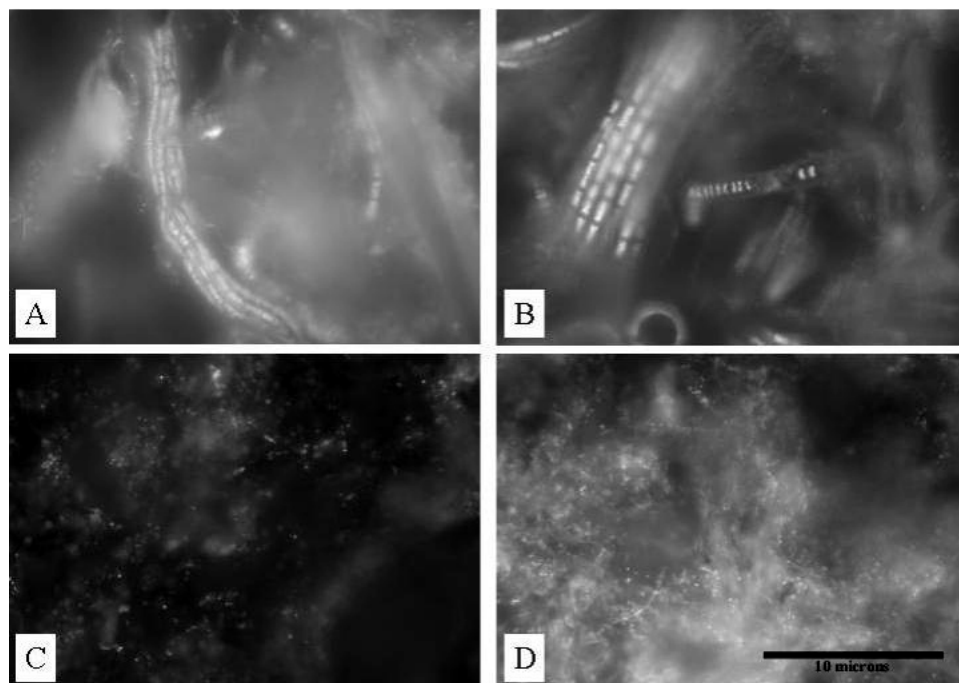


Figure 3. Fluorescent microscopy photographs of mat sections. A. 1.20 mm, B. 4.80 mm, C. 6.34 mm, D. 7.23 mm.

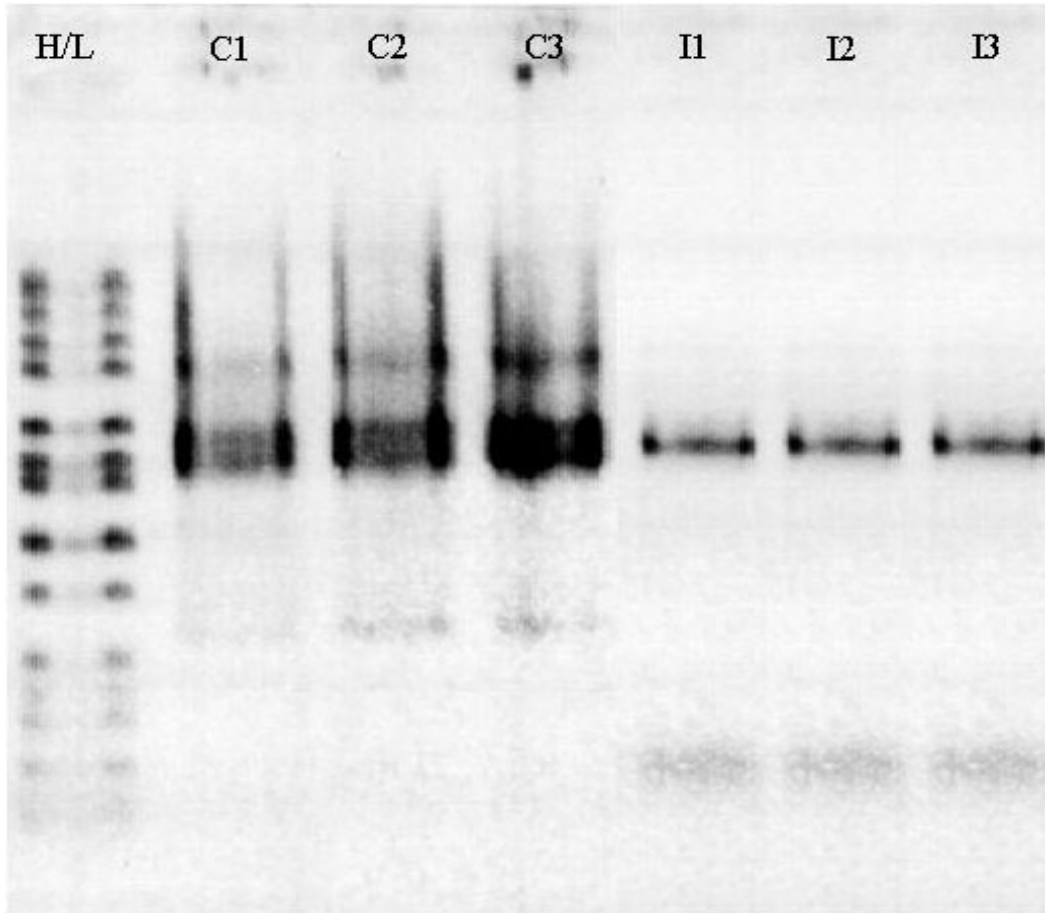


Figure 4. Reverse image of 1% Seakem gel of PCR products (using universal primers Eub A and Eub B) of CTAB (C1, C2, C3) and Isoquick (I1, I2, I3) extracts. Note streaking and multiple bands on C1, C2, and C3.

diluted accordingly prior to PCR, but rather to some unknown contaminant that caused nonspecific binding during the PCR. Although nucleic acids have been extracted from microbial mats with the use of hot phenol in previous experiments (41, 42), our comparison found the Isoquick extraction method to yield cleaner DNA, and was subsequently used to obtain the following results.

DNA fingerprints are shown in Figure 5, with each lane of the DGGE gel representing a different depth of the mat, as listed in Table II. A total of 15 different bands could be visualized throughout the profile, however as predicted by the microscopy, each independent section seems to be dominated by two bands (A & B or C & D in Figure 5). Between samples 11 and 12 (depths 3.16 and 3.41 mm), the dominant bands switch from A & B to C & D, suggesting that community composition shifts toward two different organisms, as corroborated by the pattern seen in the microscopy. The microscopy indicated a morphological shift between 4.8 and 6.34 mm, but is within 1.5 mm of the shift shown by the DGGE. The 1.5 mm disparity is most likely due to uneven mat topology and/or sample thickness. The DGGE results came from 60 μm sections while the microscopy used 20 μm sections. Bands representing organisms A & B from Figure 5 are most likely oxygenic photosynthetic cyanobacteria, similar in morphology to the organisms present in panels A & B in Figure 3. Such constituents produce O_2 and organic matter, thus propagating the oxygen gradient, and the surrounding heterotrophic bacteria. Underneath the cyanobacteria, but also exhibiting patchiness throughout the mat (40), are purple sulfur bacteria (PSB) and sulfate-reducing bacteria (SRB) (50). Bands C & D in Figure 5 and pictured in Figure 3 C & D most likely represent PSB. The PSB use H_2S to produce S_8 (S^0) and organic matter. The sink of organic matter from the cyanobacteria and PSB can then act as fuel for dissimilatory SRB, which reside in the sediments underlying the mat. The SRB use SO_4^{2-} as an electron acceptor, thus releasing H_2S . Sulfate-reducing bacteria are no longer considered to be obligate anaerobes, but have rather been found throughout the mat, including the upper layers where they are in close proximity to cyanobacteria (54, 43, 44, 51-53), and may be represented by some of the intermediate bands throughout the mat in Figure 5. Traces of A, B, C, and D can be seen at several non-adjacent depths, as is expected in a non-permanent, stratified, successional mat community. Note also several faint intermediate bands indicating the presence of other species at nearly all depths of the mat.

Conclusions

The data presented clearly show that there is a redox transition between the overlying water, the mat interior, and the underlying sediment, as expected. The transition from reduced sulfide below the mat to partially oxidized sulfide

Table II. Mat sectioning depths and subsequent sample notation. Samples not discussed in the paper yielded insufficient amounts of DNA extract and could not be processed.

Depth (mm)	Sample #						
0-0.060	1	1.86-1.92	7	3.72-3.78	13	5.58-5.64	19
0.31-0.37	2	2.17-2.23	8	4.03-4.09	14	5.89-5.95	20
0.62-0.68	3	2.48-2.54	9	4.34-4.40	15	6.2-6.26	21
0.93-0.99	4	2.79-2.85	10	4.65-4.71	16	6.51-6.57	22
1.24-1.30	5	3.1-3.16	11	4.96-5.02	17	6.82-6.88	23
1.55-1.61	6	3.41-3.47	12	5.27-5.33	18	7.13-7.19	24

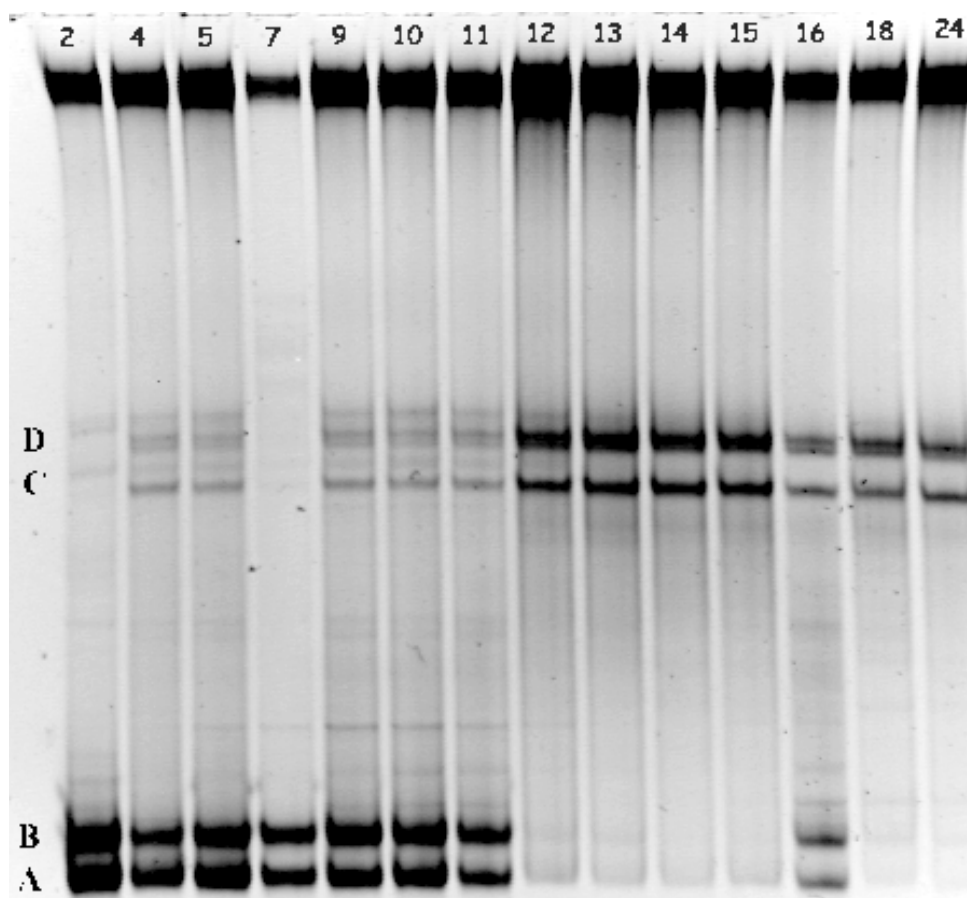


Figure 5. Reverse image of 25/55 DGGE of mat samples. Lanes are numbered by sample, as listed in Table II. Note the distinct shift from A & B to C & D between samples 11 and 12.

species (S_x^{2-}) within the mat to more oxidized sulfur species toward the top of the mat can be explained by the synergy of the chemical and biological processes occurring in the mat as described in Table III. The microscopic data corroborates the patterns present in the DGGE gel (within 1.5 mm), and both combine to form a framework for the observed chemical gradients (also within 1.5 mm). A distinct shift in microbial community is visible with microscopy between 4.8 and 6.3 mm, with DGGE between 3.16 and 3.41 mm, which corresponds to a zone of transition between $S_8/S_2O_3^{2-}$ and S_x^{2-} at 4.2 mm. The offset between each of the methods can be explained by scale. While our electrode profile and DGGE characterization were at roughly the same vertical resolution, lateral resolution could have introduced some disparity between measured chemical and biological gradients. The surface area sampled by the electrode was less than 1 mm^2 , while the $20\text{-}\mu\text{m}$ sections used for nucleotide extraction had areas of over 2 cm^2 , and were pooled to encompass a thickness of $60\text{ }\mu\text{m}$. The topography of the mat, variation in organismal stratification, and microbial patchiness all could have contributed to a biological sample less precise than the voltammetric measurements. It is also possible that the freezing of the mat introduced a change in orientation, which could account for differences between the *in situ* voltammetry and biological lab analyses.

Drawbacks to PCR-based analyses of microbial communities have been reviewed at length (55). Two major concerns lie PCR bias and different resolution capabilities of the methods. We attempted to minimize bias by using the same relative amounts of mat material per depth, using the same amount of DNA in the PCR, and using the same amount of PCR product in the DGGE. Additionally, we made comparisons between depths based on presence or absence of certain bands at certain depths, providing an overall picture of community structure shift.

Although the sediments under the mat contained significant quantities of solid phase $Fe_{(II, III)}$, as marsh sediments typically do (11), our observations suggest that iron played a very small role in the mat biogeochemistry. Solid phase $Fe_{(II, III)}$ can react with sulfide to form FeS and FeS_2 , but we did not observe a significant signal for FeS_{aq} in this mat. While the mat surface produces oxidants (O_2 and H_2O_2), which are able to oxidize sulfur compounds, PSB are able to mediate sulfide oxidation directly. The formation of S_8 and $S_2O_3^{2-}$ within the upper portions of the mat is consistent with the stronger oxidizing characteristics of that section of the mat where oxygenic photosynthesis occurs. Polysulfide formation is occurring in the interior of the mat, most likely as a result of the reaction between HS^- and the S_8 produced by PSB and GSB during anoxygenic photosynthesis. Formation of these partially oxidized sulfur species is the result of the oxidation of H_2S/HS^- which diffuses from the reducing sediments toward the overlying water. The data set is consistent with laboratory studies of sulfide oxidation (16) that show formation of polysulfides early in the

Table III. Summary of redox reactions that form chemical gradients within the microbial mat environment.

Pathway	Reaction	Contributor
Oxygenic photosynthesis	$\text{CO}_2 + \text{H}_2\text{O} \longrightarrow \text{CH}_2\text{O} + \text{O}_2$	Algae, diatoms, cyanobacteria
Anoxygenic photosynthesis	$\text{CO}_2 + 2\text{H}_2\text{S} \longrightarrow \text{CH}_2\text{O} + \text{H}_2\text{O} + 2\text{S}^0$	Cyanobacteria, purple & green sulfur bacteria
Sulfate reduction	$2(\text{CH}_2\text{O}) + \text{SO}_4^{2-} \longrightarrow 2\text{HCO}_3^- + \text{H}_2\text{S}$	Sulfur reducing bacteria
Fe chemistry	$2\text{Fe}^{3+} + \text{H}_2\text{S} \longrightarrow 2\text{Fe}^{2+} + 2\text{H}^+ + \text{S}^0 (\text{S}_x^{2-})$ $\text{Fe}^{2+} + \text{H}_2\text{S} \longrightarrow \text{FeS} + 2\text{H}^+$ $\text{FeS} + \text{H}_2\text{S} \longrightarrow \text{FeS}_2 + \text{H}_2$ $\text{Fe}^{2+} + \text{S}_x^{2-} \longrightarrow \text{FeS} + (x-1) \text{S}_8$	Chemical reaction
Sulfur oxidation	$1) 2\text{H}_2\text{S} + \mu\text{O}_2 + \text{Fe}^{2+} \longrightarrow \left\{ \begin{array}{l} \text{S}_2\text{O}_3^{2-}; \text{S}_8; \text{S}_x^{2-}; \\ \text{SO}_3^{2-}; \text{SO}_4^{2-}; \\ \text{S}_4\text{O}_6^{2-} \end{array} \right.$ $2) \text{H}_2\text{S} + \text{Fe}^{3+} \longrightarrow$	Chemical reaction, sulfur oxidizing bacteria

oxidation and production of thiosulfate later. In Figure 2 polysulfides but not thiosulfate are observed deep in the mat, and thiosulfate but not polysulfides is observed nearer the mat surface.

This was our first attempt to investigate the mat community at high resolution with both voltammetry and molecular biology techniques. Further work is ongoing, including research to produce mat-wide phylogenetic analyses to identify the organisms present, represented by individual DGGE bands. Work is also in progress to create more precise biological sampling techniques, and to provide for a more 3 dimensional profile of redox gradients. Further research is also needed to better understand the effects of the extreme diel fluctuations encountered in the mat. However, it is clear that the microelectrode technique we applied was successful in measuring discrete redox gradients, measuring the absence of dissolved metals, and therefore providing valuable information for predicting variation of the microbial constituents.

Acknowledgements

This work was supported by a grant from the National Oceanic and Atmospheric Administration (NA16RG0162-03). We would like to thank Kathy Coyne, Carol DiMeo, and Matt Cottrell for contributions to our microbial work.

References

1. Stal, L.J. *New Phytol.* **1995**, *131*, 1-32.
2. Jorgensen, B.B.; Revsbech, N.P.; Cohen, Y. *Limnol. Oceanogr.* **1983**, *28(6)* 1075-1093.
3. Van Gemerden, H. *Mar. Geol.* **1993**, *113*, 3-25.
4. Revsbech, N.P.; Jorgensen, B.B.; Brix, O. *Limnol. Oceanogr.* **1981**, *26*, 717-730.
5. Revsbech, N.P.; Jorgensen, B.B. *Limnol. Oceanogr.* **1983**, *28*, 749-756.
6. Visscher, P.T.; Beukema, J.; Van Gemerden, H. *Limnol. Oceanogr.* **1991**, *36*, 1476-1480.
7. Epping, E.H.G.; Jorgensen, B.B. *Mar. Ecol. Prog. Ser.* **1996**, *139*, 193-203.
8. Luther, G.W., III; Brendel, P.J.; Lewis, B.L.; Sundby, B.; Lefrancois, L.; Silverberg, N.; Nuzzio, D.B. *Limnol. Oceanogr.* **1998**, *43*, 325-333.
9. Brendel, P.J.; Luther, G.W., III. *Environ. Sci. Technol.* **1995**, *29*, 751-

10. Rozan, T.F.; Theberge, S.M.; Luther, G.W., III. *Anal. Chim. Acta.* **2000**, *415*, 175-184.
11. Luther, G.W., III; Glazer, B.T.; Hohmann, L.; Popp, J.I.; Taillefert, M.; Rozan, T.F.; Brendel, P.; Theberge, S.M.; Nuzzio, D.B. *J. Environ. Monit.* **2001**, *3*, 61-66.
12. Yao, W.; Millero, F.J. *Geochim. Cosmochim. Acta.* **1993**, *57*, 3359-3365.
13. Yao, W.; Millero, F.J. *Mar. Chem.* **1996**, *52*, 1-16.
14. dos Santos Afonso, M.; Stumm, W. *Langmuir.* **1992**, *8*, 1671-1675.
15. Hoffman, M.R.; *Environ. Sci. Technol.* **1977**, *11*, 61-66.
16. Chen, K.Y.; Morris, J.C. *Environ. Sci. Technol.* **1972**, *6*, 529-537.
17. Jorgensen, B.B. *Science.* **1990**, *249*, 152-154.
18. Chadwell, S.J.; Rickard, D.; Luther, G.W., III. *Aq. Geochem.* **1999**, *5*, 29-57.
19. Vairavamurthy, A.; Mopper, K. In *Biogenic Sulfur in the Environment*, Saltzmann, E.; Copper, W. J., Eds.; American Chemical Society, Washington, D.C., **1989**, vol. 393, ch. 15, pp. 231-242.
20. Lalonde, R.T.; Ferrara, L.M.; Hayes, M.P. *Org. Geochem.* **1987**, *11*, 563-571.
21. Garman, E.; Schneider, T.R. *J. Appl. Cryst.* **1997**, *30*, 211-237.
22. Porter, K.G.; Feig, Y.S. *Limnol. Oceanogr.* **1980**, *25*, 943-948.
23. Fry, J.C. In *Methods in Microbiology*, Gigorova, R. Norris, J. R., Eds.; vol. 22, Academic Press, London, pp. 41-85.
24. Bloem, J. *Mol. Microbiol. Ecol. Man.* **1995**, *4.1.8*, 1.
25. Sambrook, J.; Fritsch, E.F.; Maniatis, T. *Molecular Cloning: A Lab Manual.* **1989**.
26. Saiki, R.K.; Gelfand, D.H.; Stoffel, S.; Scharf, S.J.; Higuchi, R.; Horn, G.T.; Mullis, K.B.; Erlich, H.A. *Science.* **1988**, *239*, 487-491.
27. Medlin, L.; Elwood, H.J.; Stickel, S.; Sogin, M.L. *Gene.* **1988**, *71*, 491-499.
28. Muyzer, G.; de Waal, E.; Uitterlinden, A.G. *Appl. Environ. Microbiol.* **1993**, *59(3)*, 695-700.
29. Fischer, S.G.; Lerman, L.S. *Proc. Natl. Acad. Sci.* **1983**, *80*, 1579.
30. Luther, G.W., III; Giblin, A.E.; Varsolona, R. *Limnol. Oceanogr.* **1985**, *30*, 727-736.
31. Luther, G.W., III; Church, T.E.; Giblin, A.E.; Howarth, R.W. In *Organic Marine Geochemistry*, Sohn, M., Ed.; American Chemical Society, Washington, D.C., **1986**, vol. 305, ch. 15, pp. 231-242.
32. Batina, N.; Ciglenecki, I.; Cosovic, B. *Anal. Chim. Acta.* **1992**, *267*, 157-164.
33. Ciglenecki, I.; Cosovic, B. *Electroanalysis.* **1997**, *9*, 775-778.
34. Wang, F.A.; Buffle, J. *Limnol. Oceanogr.* **1998**, *43*, 1353-1361.

35. Jordan, J.; Talbott, J.; Yakupkovic, J. *Anal. Lett.* **1989**, *22*, 1537-1546.
36. Bond, A.M. *Modern Polarographic Methods in Analytical Chemistry*. **1980**, Marcel Dekker, New York.
37. Xu, K.; Dexter, S.C.; Luther, G.W., III. *Corrosion*. **1998**, *54*, 814-823.
38. van den Ende, F.; Van Gernerden, H. *FEMS Microbiol. Ecol.* **1993**, *13*, 69-77.
39. Visscher, P.T.; Nijurg, J.W.; Van Gernerden, H. *Arch. Microbiol.* **1990**, *155*, 75-81.
40. Paerl, H.W.; Pinckney, J.L. *Microb. Ecol.* **1996**, *31*, 225-247.
41. Teske, A.; Ramsing, N.B.; Habicht, K.; Fukui, M.; Kuver, J.; Jorgensen, B.B.; Cohen, Y. *Appl. Environ. Microbiol.* **1998**, *64*(8), 2943-2951.
42. Bateson, M.M.; Ward, D.M. *Mol. Microbiol. Ecol. Man.* **1995**, *1.1.4*, 1.
43. Jorgensen, B.B. *FEMS Microbiol. Ecol.* **1994**, *13*, 303-312.
44. Minz, D.; Fishbain, S.; Green, S.J.; Muyzer, G.; Cohen, Y.; Rittman, B.E.; Stahl, D.A. *Appl. Environ. Microbiol.* **1999**, *65*(10), 4659-4665.
45. D'Aquila, R.T.; Bechtel, L.J.; Videler, J.A.; Eron, J.J.; Gorczyca, P.; Kaplan, J.C. *Nucleic Acids Research.* **1991**, *19*, 3749.
46. Murray, A.E.; Hollibaugh, J.T.; Orrego, C. *Appl. Environ. Microbiol.* **1996**, *62*(7), 2676-2680.
47. Muyzer, G.; Teske, A.; Wirsén, C.O.; Jannasch, H.W. *Arch. Microbiol.* **1995**, *164*(3), 165-172.
48. Revsbech, N.; Jorgensen, B.B.; Blackburn, T.H. *Limnol. Oceanogr.* **1983**, *28*(6), 1062-1074.
49. Kuhl, M.; Jorgensen, B.B. *Appl. Environ. Microbiol.* **1992**, *58*, 1164-1174.
50. Ramsing, N. B.; Kuhl, M.; Jorgensen, B.B. *Appl. Environ. Microbiol.* **1993**, *59*(11), 3840-3849.
51. Canfield, D.E. and D.J. DesMarais. *Science.* **1991**, *251*, 1471-1473.
52. Frund, C. and Y. Cohen. *Appl. Environ. Microbiol.* **1992**, *58*, 70-77.
53. Visscher, P.T., Prins, R.A., Van Gernerden, H. *Appl. Environ. Microbiol.* **1992**, *86*(4), 283-293.
54. Cypionka, H. *Ann. Rev. Microbiol.* **2000**, *54*, 827-848.
55. Wintzingerode, F.V., Gbel, U.B., Stackebrandt, E. *FEMS Microbiol. Rev.* **1997**, *21*, 213-229.